Discrete-time quantum walk on complex networks for community detection

Kanae Mukai
Department of Physics, The University of Tokyo, 5-1-5 Kashiwanoha, Kashiwa, Chiba 277-8574, Japan

Naomichi Hatano*
Institute of Industrial Science, The University of Tokyo, 5-1-5 Kashiwanoha, Kashiwa, Chiba 277-8574, Japan

(Received 21 July 2019; accepted 26 May 2020; published 22 June 2020)

Many systems such as social networks and biological networks take the form of complex networks, which have a community structure. Community detection in complex networks is of great interest to many researchers in statistical physics and mathematical physics. There have been studies on community detection that use the classical random walk. The present study utilizes the discrete-time quantum walk instead. The quantum walk plays an important role in various fields, especially in research on quantum computers, and attracts much attention from mathematical physics too. The discrete-time quantum walk has two properties: it linearly spreads on a flat space, and it localizes in some cases because of quantum coherence. We demonstrate that these properties of the quantum walk are useful for community detection on complex networks. We define the discrete-time quantum walk on complex networks and utilize it for community detection. We numerically show that the quantum walk with a Fourier coin is localized in a community to which the initial node belongs. Meanwhile, the quantum walk with a Grover coin tends to be localized around the initial node, not over a community. The probability of a classical random walk on the same network converges to a uniform distribution with a relaxation time generally unknown *a priori*. We thus claim that the time average of the probability of a Fourier-coin quantum walk on complex networks reveals the community structure more explicitly than that of a Grover-coin quantum walk and a snapshot of the classical random walk. We first demonstrate our method of community detection for a prototypical three-community network, producing the correct grouping. We then apply our method to two real-world networks, namely, Zachary's karate club and the U.S. Airport network. We successfully reveal the community structure, the two communities of the instructor and the administrator in the former and major airline companies in the latter.

DOI: 10.1103/PhysRevResearch.2.023378

I. INTRODUCTION

A. Quantum walk

The quantum walk has been studied in various areas of physics. The quantum walk is divided into two types: the discrete-time quantum walk [1] and the continuous-time quantum walk [2]. The time evolution of the latter is expressed by a Hamiltonian obeying the Schrödinger equation. In the present paper, we focus on the former.

The discrete-time quantum walk is a quantum counterpart of the discrete-time classical random walk. In the classical random walk, e.g., in one dimension, a particle hops to the left or right stochastically, generating a probability distribution, whereas the quantum walk is described instead in terms of the probability amplitude of quantum superposition of the left-mover and the right-mover [1].

The quantum walk generally has the following two properties: it linearly spreads on a flat space and localizes in particular spots [3]. To be more specific, however, quantum walks with different inner states and different coin operators behave differently. The probability distribution of the three-state quantum walk in one dimension, for example, has three peaks: one that moves linearly to the left, one that moves linearly to the right, and one that localizes at the initial node [4]. The probability distribution of the two-state quantum walk in one dimension, on the other hand, has only two peaks, which spread linearly to the left and right, without any peak that localizes [5]. In the present thesis, we focus on the two-state walk, using the Fourier coin and the Grover coin [6,7]. The walks with these coin operators are called the Fourier walk and the Grover walk, respectively. We demonstrate that the two walks behave differently.

The quantum walk has been applied to quantum computers, search problems, and so on [8–10]. Many researchers consider that quantum-mechanical computers may solve problems more efficiently than their classical computers. The quantum walk has been implemented in the laboratory [11].

There have been several studies on the quantum walk on networks, mostly on regular ones [9,12]. The shift operator and the coin operator have been defined in conformity to

*hatano@iis.u-tokyo.ac.jp

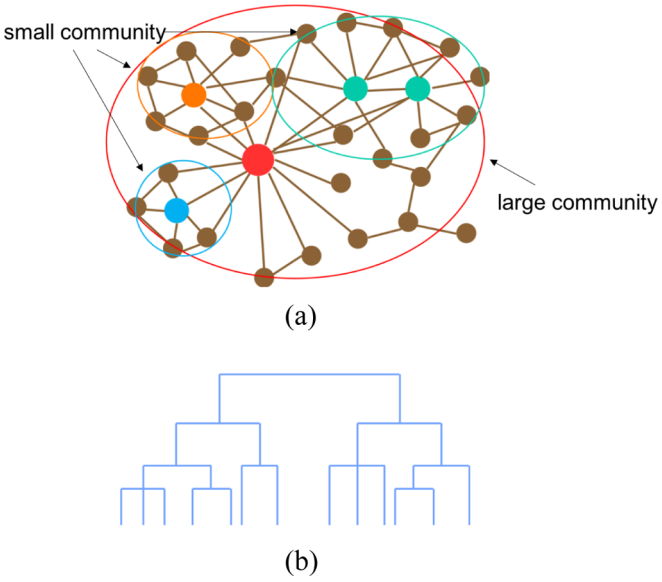

FIG. 1. (a) Schematic of the communities of a complex network arranged in a hierarchy. (b) Example of a dendrogram.

the structure of networks. The quantum walk on networks occupies an important role in search problems. In general, it takes classical algorithms $O(N)$ steps to identify the target record from an unsorted database of N records, while it takes quantum mechanical systems only $O(\sqrt{N})$ steps [8].

B. Complex networks

Many systems including social networks and biological networks have been found to have distinctive features drastically different from random graphs and, hence, are collectively called complex networks [13–16]. Representative examples include acquaintance networks [17], the World Wide Web [18], corporate transaction networks [19], neural networks [20], food webs [21], and metabolic networks [22].

The distinctive features of the complex networks often quoted include the scale-free property and the small-world effect, although there are so-called complex networks that do not have these features. The former feature means that the histogram of the degrees of the nodes (the number of links attached to a node) follows a power-law behavior [23]; in other words, there are a large number of nodes with low degrees and a small number of nodes with high degrees in a self-similar way. The latter feature means that the average distance between a randomly chosen pair of nodes in a complex network is surprisingly shorter than that in a random network [24].

These features may indicate that many complex networks have a hierarchical structure; see Fig. 1, for example. When we depict the structure as a tree, which is called a dendrogram in the social sciences [25] [see Fig. 1(b), for example], the leaves correspond to the nodes and the branches to the links. Nodes in higher levels of the dendrogram can have more links to nodes in lower levels in a self-similar way. A node in one branch of the dendrogram to another node in a different branch can be connected by a short path through nodes in higher levels.

In a hierarchical complex network, we should be able to find communities in various levels. The community is a subset of nodes within the network such that connections among the nodes of the community are denser than those among the other nodes [25]. As the hierarchy in Fig. 1 suggests, a node at a high level of the dendrogram is likely to be at the center of each community typically with many links, which we call a hub. It is therefore of great importance for detecting the features of complex networks to identify communities.

There are several algorithms for community detection [13,25–28]. The conventional method is the hierarchical clustering [13,25,26,29]. In this method, one calculates a weight $W_{i,j}$ for every pair of nodes in the network. The weight shows how closely connected the nodes are. Starting from the nodes with no links between them, one adds links between pairs in the order of their weights. The nodes are classified into communities, and the communities are grouped into larger communities. Many different weights have been proposed in this algorithm. The weight considering the paths longer than the shortest ones was taken into account in Ref. [30]. Another method is called the divisive algorithm [13]. Starting from the whole network, one cuts the links. The network is divided into smaller subnetworks, which are identified as communities. Another research presents an algorithm with a modularity [26,27,31,32]. The modularity is a property of a network and a division of the network into communities. If there are many links within the communities and a few links between the communities, the division is good.

There have been several studies on community detection that used discrete-time classical random walks [28,33]. These approaches are based on the consideration that random walks on the networks tend to get trapped within the communities [28]. One computes the frequency at which each node is visited by a random walker and explores possible partitions by using deterministic algorithms [33].

We here utilize the discrete-time *quantum* walk instead for community detection. The infinite-time average of the transition probability, normalized by the number of links, of the Fourier-coin quantum walk on a complex network shows localization in a community and, thereby, reveals the community structure. The Grover-coin quantum walk, in contrast, tends to be localized around the initial node, presumably due to the localized eigenstates of the time-evolution unitary with degenerate ± 1 eigenvalues. For the classical random walk on the same network, the probability converges to a flat distribution as time passes. Although the community structure partially emerges before the convergence, it is generally *a priori* unknown which time step of the walk is best for the community detection. We thus claim that the Fourier-coin quantum walk on complex networks reveals the community structure more explicitly than the Grover-coin quantum walk and the classical random walk.

II. QUANTUM WALK ON COMPLEX NETWORKS

We first describe our definition of the quantum walk on complex networks. It requires a node-dependent coin operator because each node generally has a different number of links.

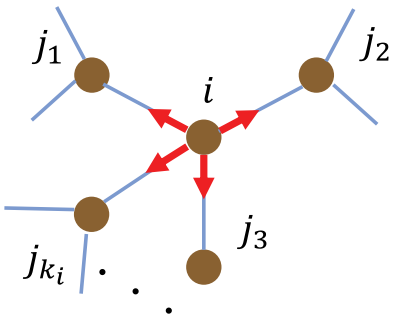

FIG. 2. Definition of a quantum state in complex networks.

We define the quantum state in a complex network (see Fig. 2, for example) in the form

$$|\psi(t)\rangle = \sum_{i=1}^{N} \sum_{j=1}^{k_i} \psi_{i,j}(t)|i \to j\rangle, \tag{1}$$

where N is the total number of nodes, state $|i \to j\rangle$ resides on node i and is about to hop to the adjacent node j on a link connecting i and j, and k_i is the number of links attached to node i. The total Hilbert space $\mathcal{H} = \mathcal{H}_1 \oplus \mathcal{H}_2 \oplus \ldots \oplus \mathcal{H}_N$ consists of the Hilbert space of each node $\mathcal{H}_i$, which is spanned by $(|i \to j_1\rangle, |i \to j_2\rangle, \ldots, |i \to j_{k_i}\rangle)$. The dimensionality of the total Hilbert space is therefore given by

$$D = \sum_{i=1}^{N} k_i, \tag{2}$$

which is the total number of links under double-counting. We normalize state $|\psi(t)\rangle$ as in

$$\langle\psi(t)|\psi(t)\rangle = \sum_{i=1}^{N} \sum_{j=1}^{k_i} |\psi_{i,j}(t)|^2 = 1. \tag{3}$$

We can write the probability of the existence on a node i at time t as

$$p(i;t) = \sum_{j=1}^{k_i} |\psi_{i,j}(t)|^2. \tag{4}$$

The time evolution of state $|\psi(t)\rangle$ is given by

$$|\psi(t)\rangle = U|\psi(t-1)\rangle \tag{5}$$

$$= U^t|\psi(0)\rangle, \tag{6}$$

where the unitary operator U is the product of a shift operator S and a coin operator C:

$$U = SC. \tag{7}$$

We define the shift operator $S : \mathcal{H} \to \mathcal{H}$ by

$$S|i \to j\rangle = |j \to i\rangle. \tag{8}$$

The choice of this shift operator may appear to be atypical compared to the one defined for a one-dimensional lattice, but it is necessary because of the existence of dangling bonds. When node j is at the end of a dangling bond as the bottom one $i \to j_3$ in Fig. 2, Eq. (8) is the only possible choice. Indeed, it has been used for searching a marked vertex on a specific graph called the Cayley tree [9]. We can also easily prove that the shift operator of Eq. (8), if defined on a one-dimensional lattice, can be mapped to the standard shift operator by introducing an extra factor to the coin operator; see Appendix A.

We define the coin operator C by

$$C = C_1 \oplus C_2 \oplus \ldots \oplus C_N, \tag{9}$$

where we first set the coin operator of a node i, $C_i : \mathcal{H}_i \to \mathcal{H}_i$, as

$$C_i^{\mathrm{F}} \begin{pmatrix} |i \to j_1\rangle \\ |i \to j_2\rangle \\ |i \to j_3\rangle \\ \vdots \\ |i \to j_{k_i}\rangle \end{pmatrix} = \frac{1}{\sqrt{k_i}} \begin{pmatrix} 1 & 1 & 1 & \cdots & 1 \\ 1 & e^{i\theta/k_i} & e^{2i\theta/k_i} & \cdots & e^{(k_i-1)i\theta/k_i} \\ 1 & e^{2i\theta/k_i} & e^{4i\theta/k_i} & \cdots & e^{2(k_i-1)i\theta/k_i} \\ \vdots & \vdots & \vdots & \ddots & \vdots \\ 1 & e^{(k_i-1)i\theta/k_i} & e^{2(k_i-1)i\theta/k_i} & \cdots & e^{(k_i-1)(k_i-1)i\theta/k_i} \end{pmatrix} \begin{pmatrix} |i \to j_1\rangle \\ |i \to j_2\rangle \\ |i \to j_3\rangle \\ \vdots \\ |i \to j_{k_i}\rangle \end{pmatrix} \tag{10}$$

with $\theta = 2\pi$. (Note that the numbering of the neighboring nodes $\{j_1, j_2, \ldots, j_{k_i}\}$ is arbitrary but does affect the dynamics.) This specific operator is called the Fourier coin [7] because it is a Fourier matrix. The Fourier-coin quantum walk (the Fourier walk) has been used on a particular kind of network [34].

Below we also consider the quantum walk with an alternative coin operator, namely, the Grover coin [6], which is given by

$$C_i^{\mathrm{G}} \begin{pmatrix} |i \to j_1\rangle \\ |i \to j_2\rangle \\ |i \to j_3\rangle \\ \vdots \\ |i \to j_{k_i}\rangle \end{pmatrix} = \frac{1}{k_i} \begin{pmatrix} 2-k_i & 2 & 2 & 2 & 2 \\ 2 & 2-k_i & 2 & 2 & 2 \\ 2 & 2 & 2-k_i & 2 & 2 \\ \vdots & \vdots & \vdots & \ddots & \vdots \\ 2 & 2 & 2 & \cdots & 2-k_i \end{pmatrix} \begin{pmatrix} |i \to j_1\rangle \\ |i \to j_2\rangle \\ |i \to j_3\rangle \\ \vdots \\ |i \to j_{k_i}\rangle \end{pmatrix}. \tag{11}$$

This is called the Grover matrix, being related to Grover's search algorithm [35]. There are many studies on the Grover-coin quantum walk (Grover walk). The periodicity of the Grover walk on some finite graphs has been clarified [36]. We show that the Fourier coin works much better than the Grover coin for the purpose of community detection.

We prepare the initial state for the quantum walk as a state in which a specific state on a specific node i_{start}, $|i_{\mathrm{start}} \to j\rangle$, has the element unity and the others have elements 0. In Sec. III, we take the average over the adjacent nodes j as shown in (13) below.

III. COMMUNITY DETECTION

A. Infinite-time average

We numerically show hereafter that the probability of a Fourier walk becomes higher in hubs as time passes whichever node we choose as the initial one $i_{\rm start}$. We can thus detect hubs of complex networks, although the threshold to detect them is an open question. We also show that the state of the Fourier walk on complex networks is localized in a community of the initial node and, thereby, reveals the community structure. For a quantum walk on a one-dimensional finite lattice, the probability distribution after a long period of time has been proved to be stationary and uniform when the quantum walk behaves symmetrically [37]. For a quantum walk on a complex network, on the other hand, we here show that the infinite-time average of the normalized transition probability, calculated from the eigenvectors, shows localization.

Let us calculate the infinite-time average of the transition probability by expanding the unitary operator $U = SC$ in terms of its eigenstates,

$$U = \sum_{\mu=1}^{D} |\mu\rangle e^{i\theta_\mu} \langle\mu|, \tag{12}$$

where $|\mu\rangle$ is the eigenvector and $e^{i\theta_\mu}$ is its eigenvalue with a real argument θ_μ. The transition probability that the quantum walk starting from a node i reaches a node l is given by

$$p(i \to l; t) = \frac{1}{k_i} \sum_{m=1}^{k_l} \sum_{j=1}^{k_i} |\langle l \to m|U^t|i \to j\rangle|^2, \tag{13}$$

where $|i \to j\rangle$ is the initial state and $|l \to m\rangle$ is the state at step t. The factor $1/k_i$ is to average over direction j of the initial state. We also took the summation over direction m of the final state.

The infinite-time average of the transition probability is given by

$$\overline{p(i \to l)} = \lim_{T\to\infty} \frac{1}{T} \frac{1}{k_i} \sum_{t=0}^{T-1} \sum_{m=1}^{k_l} \sum_{j=1}^{k_i} |\langle l \to m|U^t|i \to j\rangle|^2 \tag{14}$$

$$= \frac{1}{k_i} \sum_{\mu=1}^{D} \sum_{m=1}^{k_l} \sum_{j=1}^{k_i} |\langle l \to m|\mu\rangle|^2 |\langle\mu|i \to j\rangle|^2, \tag{15}$$

where we have assumed

$$\lim_{T\to\infty} \frac{1}{T} \sum_{t=0}^{T-1} e^{i(\theta_\mu - \theta_\nu)t} = \delta_{\mu\nu}, \tag{16}$$

which is valid if the eigenvalues are nondegenerate and distributed almost randomly over the unit circle. In this case, the quantum walk on the network is a superposition of oscillation with various frequencies, and hence the infinite-time average makes sense.

In order to check the validity of the formulation, we show in Figs. 3(b) and 3(c) the eigenvalue distributions of the time-evolution unitary matrix U for the Fourier walk and the Grover walk on the prototypical three-community network given in Fig. 3(a), for which $N = 21$ and $D = 78$. In both cases, the 78 eigenvalues are distributed over a unit circle on the complex plane. The eigenvalues of the Fourier walk are nondegenerate, while almost half of the eigenvalues of the Grover walk are degenerate at either $+1$ or -1. (Precisely, the degeneracies are 20 and 18 for the eigenvalues ± 1, respectively.) The histogram in Fig. 3(d) shows more clearly that the eigenvalues of the Fourier walk are distributed much more evenly over the unit circle than the eigenvalues of the Grover walk. We thus realize that the Fourier walk is more suitable for formulation (15) than the Grover walk.

It has been proven for the Grover walk that the eigenvectors of the eigenvalues degenerate to ± 1 are localized on loops of graphs [38]; indeed the degree of the degeneracy is completely determined by the topology of the graph (see Appendix B for tutorial examples). On regular graphs, this degeneracy would lead to a proof of the localization on the initial node after linear combination of the eigenvectors on the loops [38]. We numerically show below that the Grover walk on a graph is also localized around the initial node of the walk.

Figure 4(a) shows the infinite-time average of the probability of the Fourier walk on the three-community network in Fig. 3(a), computed according to Eq. (15) based on the numerical diagonalization of U. The vertical axis shows the initial node i, the horizontal axis shows the target node l, and each square color-codes the amplitude of the time-averaged probability $\overline{p(i \to l)}$; note that the probabilities are roughly proportional to the number of links, and those of the hubs (nodes 1, 13, and 21) are the highest. We can thus identify hubs clearly from the infinite-time average of the probability.

Based on the observation in Fig. 4(a), we define the *normalized* probability $P(i \to l; t)$ of each node by dividing the probability $p(i \to l; t)$ by the number of links of the target node l:

$$P(i \to l; t) = \frac{p(i \to l; t)}{k_l} = \frac{1}{k_l k_i} \sum_{m=1}^{k_l} \sum_{j=1}^{k_i} |\langle l \to m|U^t|i \to j\rangle|^2. \tag{17}$$

The infinite-time average of the normalized probability is given by

$$\overline{P(i \to l)} = \frac{\overline{p(i \to l)}}{k_l} = \lim_{T\to\infty} \frac{1}{T} \frac{1}{k_l k_i} \sum_{t=0}^{T-1} \sum_{m=1}^{k_l} \sum_{j=1}^{k_i} \left|\langle l \to m|U^t|i \to j\rangle\right|^2 \tag{18}$$

$$= \frac{1}{k_l k_i} \sum_{\mu=1}^{D} \sum_{m=1}^{k_l} \sum_{j=1}^{k_i} |\langle l \to m|\mu\rangle^2 |\langle\mu|i \to j\rangle|^2. \tag{19}$$

This infinite-time average then becomes symmetric with respect to the exchange of l and i as in $\overline{P(i \to l)} = \overline{P(l \to i)}$.

Figure 4(b) color-codes the infinite-time average of the *normalized* probability $\overline{P(i \to l)}$ calculated from the eigenvectors of the Fourier walk for the three-community network in Fig. 3(a). The normalized transition probability between the initial node and the other nodes in the same community is high, which reveals the community structure.

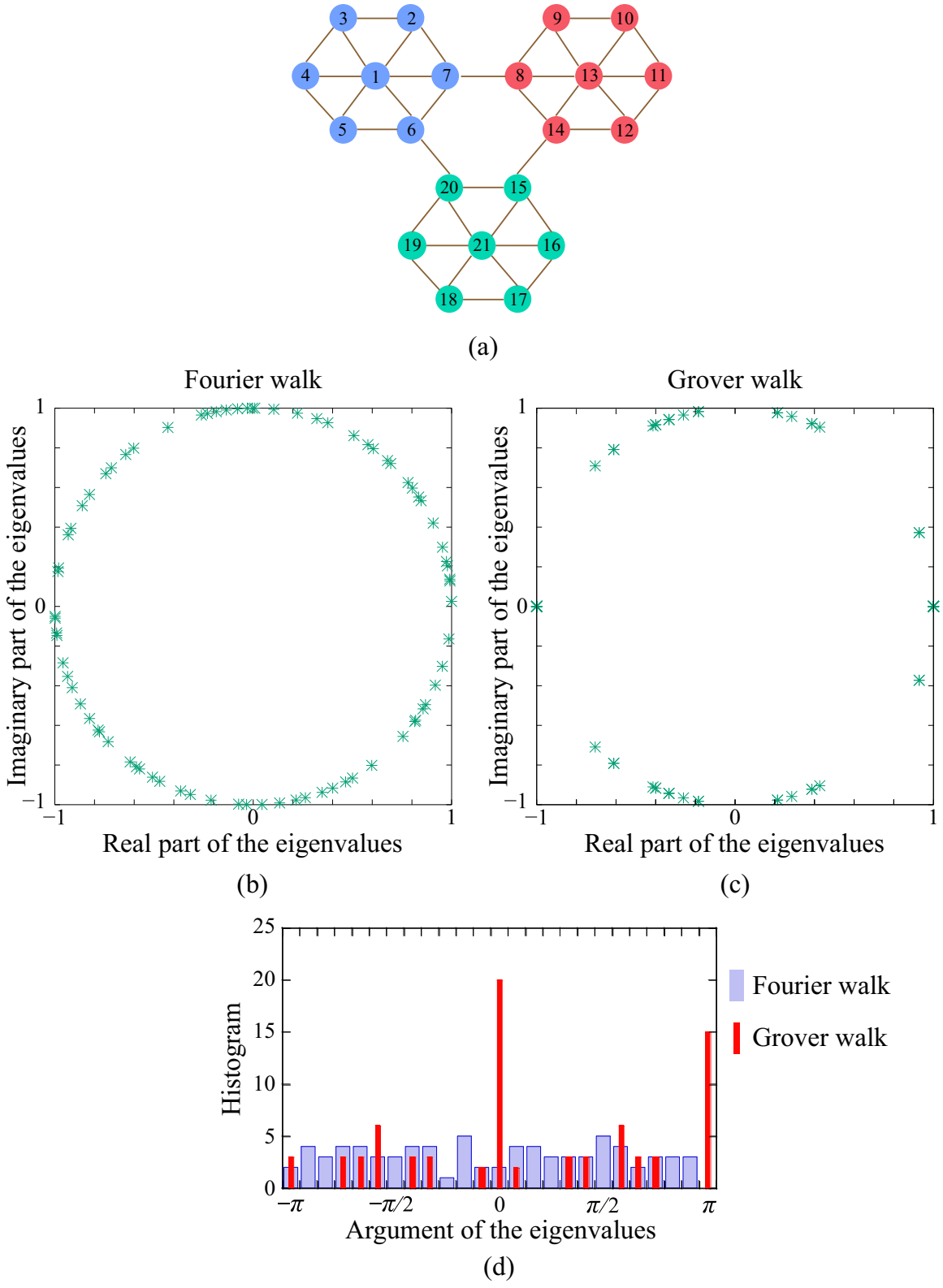

FIG. 3. (a) A prototypical three-community network, for which $N = 21$ and $D = 78$. The hubs are nodes 1, 13, and 21. (b, c) Complex eigenvalues of the time-evolution unitary matrix U for (b) the Fourier walk and (c) the Grover walk on the three-community network in (a). The horizontal axis shows the real part and the vertical axis shows the imaginary part of the eigenvalues. There are 78 eigenvalues plotted because $D = 78$. Within the numerical double-precision, the unitary matrix of the Fourier walk has no degeneracy in (b), whereas for that of the Grover walk, the eigenvalues ± 1 have the degeneracy 20 and 18, respectively, in (c). (d) Distribution of the argument of the eigenvalues for the Fourier walk (wide blue columns) and for the Grover walk (narrow red columns).

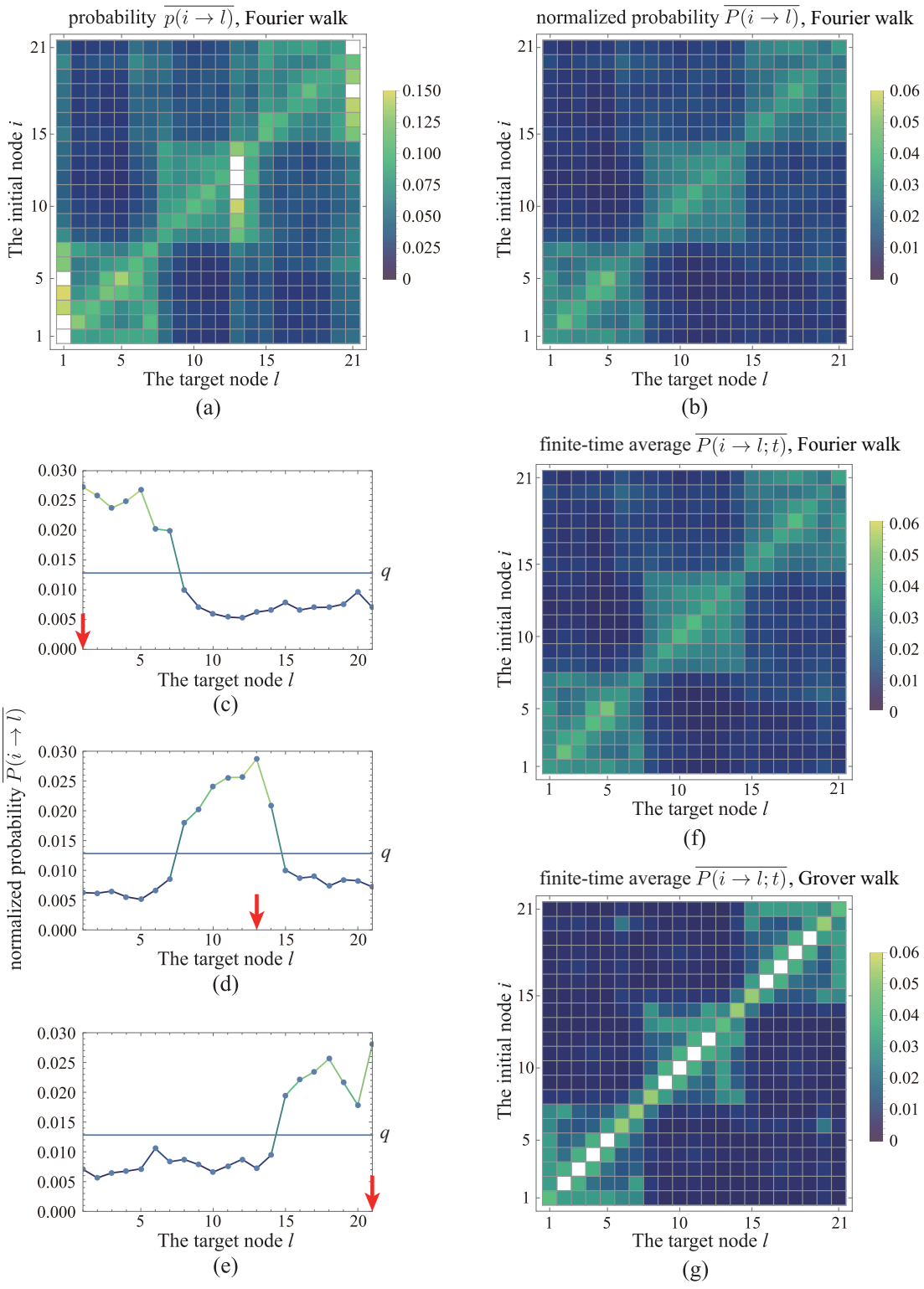

FIG. 4. (a) Infinite-time average, (15), of the probability $\overline{p(i \to l)}$ of the Fourier walk on the three-community network in Fig. 3(a). (b) Infinite-time average of the *normalized* probability $\overline{P(i \to l)}$ in Eq. (19) of the Fourier walk on the three-community network. In (b) and (c), the vertical axis shows the initial node i and the horizontal axis shows the target node l, while each square indicates the value of either $\overline{p(i \to l)}$ or $\overline{P(i \to l)}$. A white square indicates a value off scale in the higher direction. (c–e) Infinite-time average of the normalized probability $\overline{P(i \to l)}$ in Eq. (19) of the Fourier walk on the three-community network that starts from the hub $i = 1$ (c), the hub $i = 13$ (d), and the hub $i = 21$ (e), each of which is indicated by a red arrow. The horizontal axis shows the target node l and the vertical axis shows the normalized probability $\overline{P(i \to l)}$ with $i = 1, 13, 21$. The horizontal line in the middle indicates the threshold $q = 1/78 \simeq 0.0128$. (f) Time average of the normalized probability $P(i \to l;t)$ over the first 100 steps of the Fourier walk on the three-community network. (g) The same as (f), but for the Grover walk.

Figures 4(c)–4(e) show the same quantity as in Fig. 4(b), but only for cases in which the walk starts from the hubs [nodes $i = 1$, 13, and 21, which are indicated by red arrows in Figs. 4(c)–4(e)]. In order to detect the community structure quantitatively, we here tentatively define the threshold for the detection of a community to be $q = 1/D$, where $D = 78$, which is indeed the stationary probability normalized by the number of links k_l of the *classical* random walk on the network.

We thereby define a community as follows:

(i) We first define a hub i as a node with the highest order k_i.

(ii) If the normalized probability starting from hub i to a node l is greater than the threshold q, namely, if

$$\overline{P(i \to l)} > q, \tag{20}$$

node l is a member of the community of hub i.

This algorithm clearly reveals the three communities of the three-community network in Fig. 3(a). For instance, if the Fourier walk starts from hub 1 as in Fig. 4(b), the probability of nodes 2, 3, 4, 5, 6, and 7, which belong to the same community, is higher than the threshold q. We can thus successfully identify which community each node belongs to.

In order to justify the algorithm from a different perspective, we show that the Fourier walk on the network is localized in a community to which the initial node belongs. Let us evaluate the localization of the eigenvectors using the inverse participation ratio (IPR) [39,40]. The IPR of an eigenvector

$$|\mu\rangle = \sum_{l=1}^{N} \sum_{m=1}^{k_l} \psi_\mu(l,m)|l \to m\rangle \tag{21}$$

is given by

$$\mathrm{IPR}(\mu) = \frac{\sum_{l=1}^{N} p_\mu(l)^2}{\left(\sum_{l=1}^{N} p_\mu(l)\right)^2} = \sum_{l=1}^{N} p_\mu(l)^2, \tag{22}$$

where the probability $p_\mu(l)$ is

$$p_\mu(l) = \sum_{m=1}^{k_l} |\psi_\mu(l,m)|^2 \tag{23}$$

with the normalization $\sum_{l=1}^{N} p_\mu(l) = 1$ for all μ.

If the eigenvector is sharply localized to one node, the IPR is close to unity. If the eigenvector is delocalized, the IPR is as small as $1/N$, which is $1/21 \approx 0.0476$ in the present case of the three-community network in Fig. 3(a). If the eigenvector were localized uniformly in one of the communities of the network as in

$$p_\mu(l) = \begin{cases} \frac{1}{7} & \text{for } l = 1, 2, \ldots, 7, \\ 0 & \text{otherwise,} \end{cases} \tag{24}$$

the IPR would be exactly $1/7 \approx 0.14$.

Figure 5(a) shows the IPR of each eigenvector for the Fourier walk on the three-community network. We find that all states have an IPR higher than $1/21 \simeq 0.047\,62$ [the thinner horizontal line in Fig. 5(a)] and several eigenvectors are localized more strongly than the IPR $= 1/7 \simeq 0.1429$ [thicker horizontal line in Fig. 5(a)]. The naive average of the IPR over all eigenstates is about $0.1151 \simeq 1/8.7$, which is not far from $1/7$.

Figure 5(b), on the other hand, shows the *normalized* probability

$$P_\mu(l) = \frac{p_\mu(l)}{k_l} \tag{25}$$

of the Fourier walk on the three-community network. The probability distribution for each eigenvalue shows the localization, often over a community. For the probability distribution for eigenstate number 1 (for which the IPR is about 0.150), for instance, the probability for node 1 and the nodes in the same community (from $l = 1$ to $l = 7$) is visibly higher than that for the other nodes; in other words, this eigenvector is localized in the first community. Similarly, the probability distribution of eigenstate number 46 (for which the IPR is about 0.137) is localized in the second community, and that of eigenstate number 11 (for which the IPR is about 0.135) is localized in the third one.

The localization of the quantum walk may be related to the Anderson localization. In the standard sense, the Anderson localization is the property of quantum particles in random media [41,42]. There are several studies on the Anderson localization of the discrete-time quantum walk on lattices with randomness [43,44]. The quantum walk on the complex network may be similar to the quantum particle in random media because of the inhomogeneity of the network and, hence, may experience the Anderson localization.

B. Finite-time calculation

We next present our finite-time results for the quantum walk on the same three-community network in Fig. 3(a). We operated the unitary matrix U to the initial state $|i \to j\rangle$ up to 100 steps and averaged the resulting probability over j.

Figure 4(f) shows the time average of the normalized probability $\overline{P_t(i \to l)}$ over 100 steps, from $t = 1$ through $t = 100$. It is almost the same as Fig. 4(b), also revealing the community structure. The fact that the finite-time average is almost equal to the infinite-time average is presumably thanks to the property of the quantum walk that the front of the probability spreads linearly. This implies that we can apply the present method to complex networks which are too large to diagonalize the time-evolution unitary matrix U by computing a finite-time average instead of the infinite-time average.

Figure 4(g), on the other hand, shows the same time average of the normalized probability $\overline{P(i \to l; t)}$, but for the *Grover* walk. We can see that the diagonal elements are much larger than the other elements. In other words, the Grover walk mostly stays at the initial node through the 100 steps, implying strong localization at each node.

We may relate this phenomenon to findings for the Grover walk on regular lattices [38,45,46]. As mentioned in Sec. III A, it has been proven that any eigenvectors with degenerate eigenvalues ± 1 of the unitary matrix of the Grover walk on regular lattices are broken down to states localized on loops, which leads to a proof of the localization of the walk on the initial node. This may also be the case in the present three-community network. Indeed, the localization numerically demonstrated in Fig. 1(a) of Ref. [45] resembles

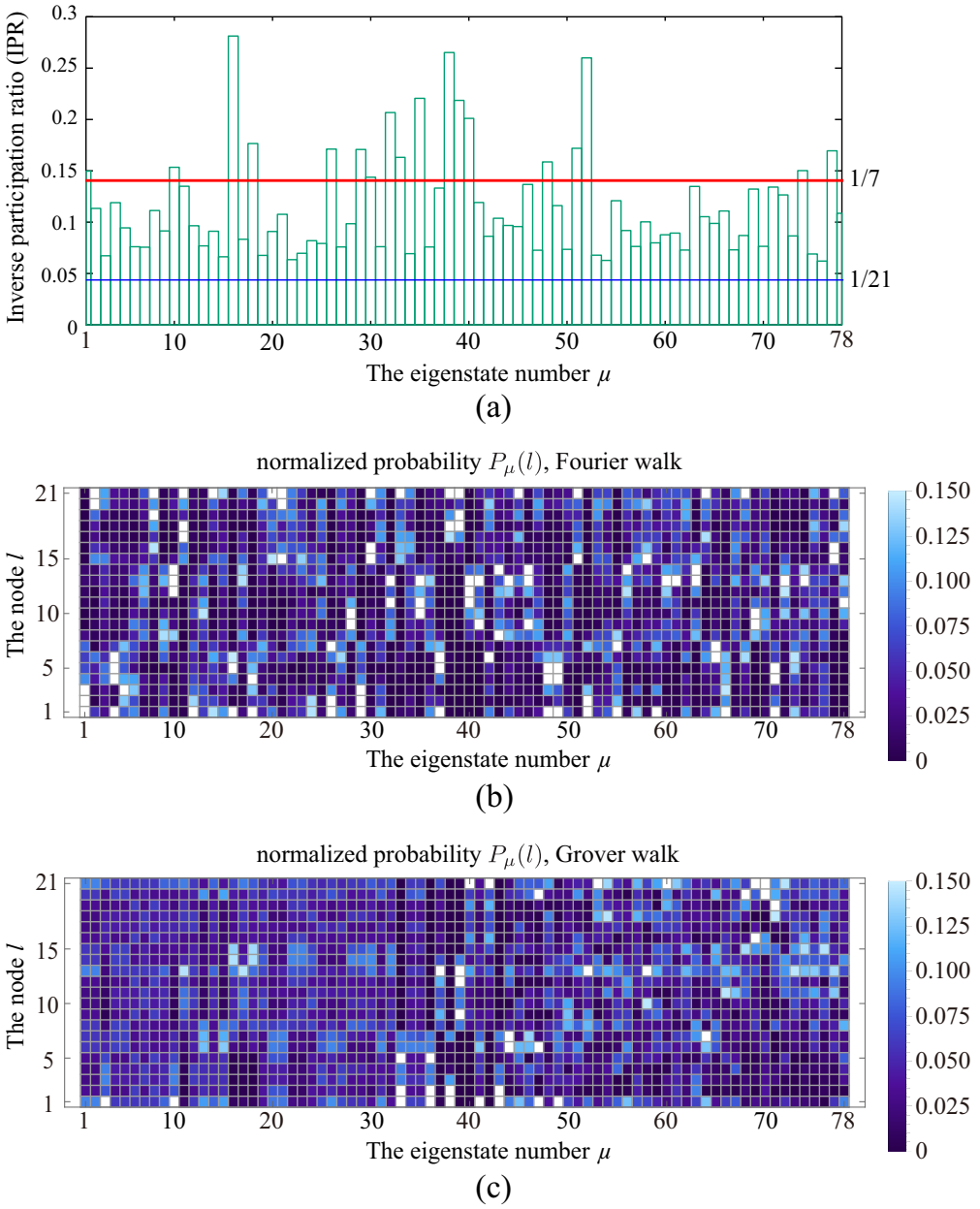

FIG. 5. (a) Inverse participation ratio (IPR) of each eigenvector for the Fourier walk on the three-community network. The horizontal axis shows the eigenstate number μ and the vertical axis shows the IPR of each eigenstate. The thin blue horizontal line indicates the IPR value $1/21$, which corresponds to a uniformly extended state, while the thick red horizontal line indicates the IPR value $1/7$, which corresponds to a state uniformly localized in one of the three communities. (b) *Normalized* probability $P_\mu(l)$ in Eq. (25) calculated from the eigenstates for the Fourier walk on the three-community network. The horizontal axis shows the eigenstate number μ and the vertical axis shows node l, while each square indicates the value of $P_\mu(l)$. (c) The same as (b), but for the Grover walk.

the behavior of the diagonal concentration in Fig. 4(g) here. Figure 5(c) also shows that the normalized probability $P_\mu(l)$ in Eq. (25) calculated from the eigenstates for the Grover walk are localized in nodes rather than in communities if the eigenvalue is ± 1 (eigenstate numbers 41 to 78). For example, states 41, 44, 47, 49, and so on, have small elements in a community but are mostly localized to one or a couple of nodes.

Figure 6 shows the first few steps in the time evolution $P(i \to l; t)$ of the Fourier and Grover walks that started from various initial nodes i. When a walk starts from node 1 of the three-community network in Fig. 3(a), the Fourier walk [Fig. 6(a)] spreads over the first community in a couple of steps and stays so afterwards. On the other hand, the Grover walk [Fig. 6(b)], although it has higher probabilities over the first community than the rest, shows some oscillation in time and has an even higher probability at the initial node 1 from time to time. When a walk starts from node 7, the Fourier walk [Fig. 6(c)] again spreads over the first community in a few steps and stays so afterwards. The Grover walk [Fig. 6(d)], however, has high probabilities on nodes 7, 6, and 2.

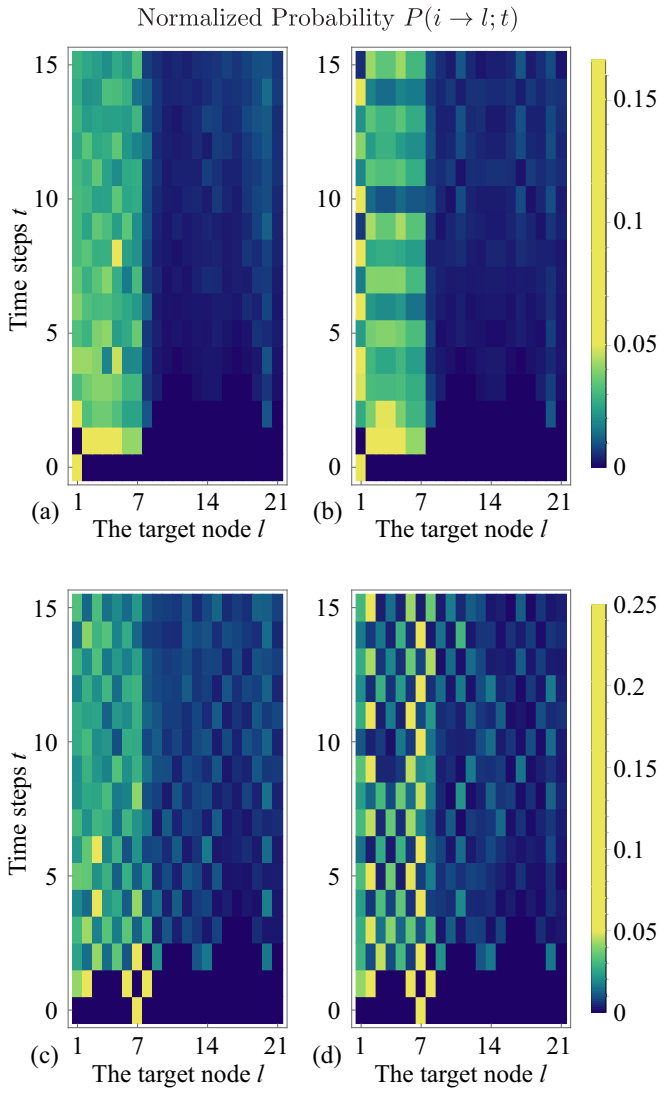

FIG. 6. Time evolution on the three-community network of the normalized probability $P(i \to l;t)$ from $t = 0$ to $t = 15$ for (a) the Fourier walk with $i = 1$, (b) the Grover walk with $i = 1$, (c) the Fourier walk with $i = 7$, and (d) the Grover walk with $i = 7$.

To summarize, the time evolution of the Fourier walk tends to get localized over a community whichever node it starts from, while that of the Grover walk tends to get localized on a couple of nodes around the initial one. Therefore, the Fourier walk reveals the community structure more clearly than the Grover walk.

Finally, we compare the probability of the quantum walk to that of the classical random walk on the same network. The probability of the classical random walk eventually relaxes to a flat distribution, which is equal for all nodes, and hence the infinite-time average of the probability does not reveal the community structure. For community detection we would have to choose a specific time step, which is unknown *a priori*. We thus claim that using the time average of the probability of the quantum walk is a more tractable way of community detection than trying to find a specific time step of the classical random walk.

IV. APPLICATION TO REAL-WORLD NETWORKS

A. Zachary's karate-club network

Let us apply the above algorithm of the community detection to Zachary's karate-club network [17] [Fig. 7(a)], which is a friendship network in a karate club in a university in the United States. The club split into two communities, one clustered around the instructor (node 1) and the other around the administrator (node 34). In Zachary's psychological experiment, each member of the club answered his or her friends' names and the community to which he or she belongs.

The network in Fig. 7(a), for which the total number of nodes is $N = 34$ and the total number of links is $D = 156$, is based on the first set of answers. The hubs of this network are nodes 1 and 34. The second set of answers tells us that the communities are as follows:

Group of node 1: 1, 2, 3, 4, 5, 6, 7, 8, 11, 12, 13, 14, 17, 18, 20, 22 [red squares in Fig. 7(a)].

Group of node 34: 9, 10, 15, 16, 19, 21, 23, 24, 25, 26, 27, 28, 29, 30, 31, 32, 33, 34 [blue circles in Fig. 7(a)].

In this sense, this is a rare case of the complex network for which the 'correct' answer of the community detection is known, although the correctness can be disputed; see the last paragraph of the present section. We show that our method 'correctly' identifies the two communities.

Figure 7(b) indicates that the eigenvalues for the Fourier walk, which we computed by numerical diagonalization of the 156×156 matrix, distributes quite evenly on the unit circle. We confirmed that there is no degeneracy within the numerical double-precision. This guarantees the computation of the infinite-time average given in Sec. III A to be valid for the karate-club network too. Figure 7(c) shows the infinite-time average of the probability in Eq. (15), which we computed from the numerical diagonalization. The probabilities of nodes 1 and 34 are higher than those of any other nodes. We can clearly identify nodes 1 and 34 as the hubs in this figure.

Figures 7(d) and 7(e) show the infinite-time average of the *normalized* probabilities, (19), of the Fourier walk which starts from the hubs [nodes 1 and 34, which are indicated by red arrows in Figs. 7(d) and 7(e)]. Let us again tentatively define the threshold as $q = 1/D$, where $D = 156$. The nodes whose probabilities are higher than the threshold q belong to the community in which the initial node is the hub. For instance, if the Fourier walk starts from hub 1, the probability of node 2, which belongs to the same community, is higher than the threshold q. We can thus detect which community each node belongs to.

Figures 7(f) and 7(g) show the time evolution of the normalized probabilities, (17), of the Fourier walk that starts from nodes 1 and 34. Here the nodes in the first community are gathered on the left, and those in the second community on the right. We can clearly see that the walk spreads over the respective community in the first couple of steps in the time evolution.

Comments are in order here; the detection of nodes 3 and 20 [highlighted by the dotted arrow in Fig. 7(a)] is quite marginal. First, for node 20, the normalized probabilities $\overline{P(1 \to 20)}$ and $\overline{P(34 \to 20)}$ are both greater than the threshold $q = 1/D$. Nonetheless, the former, $\overline{P(1 \to 20)} \simeq$

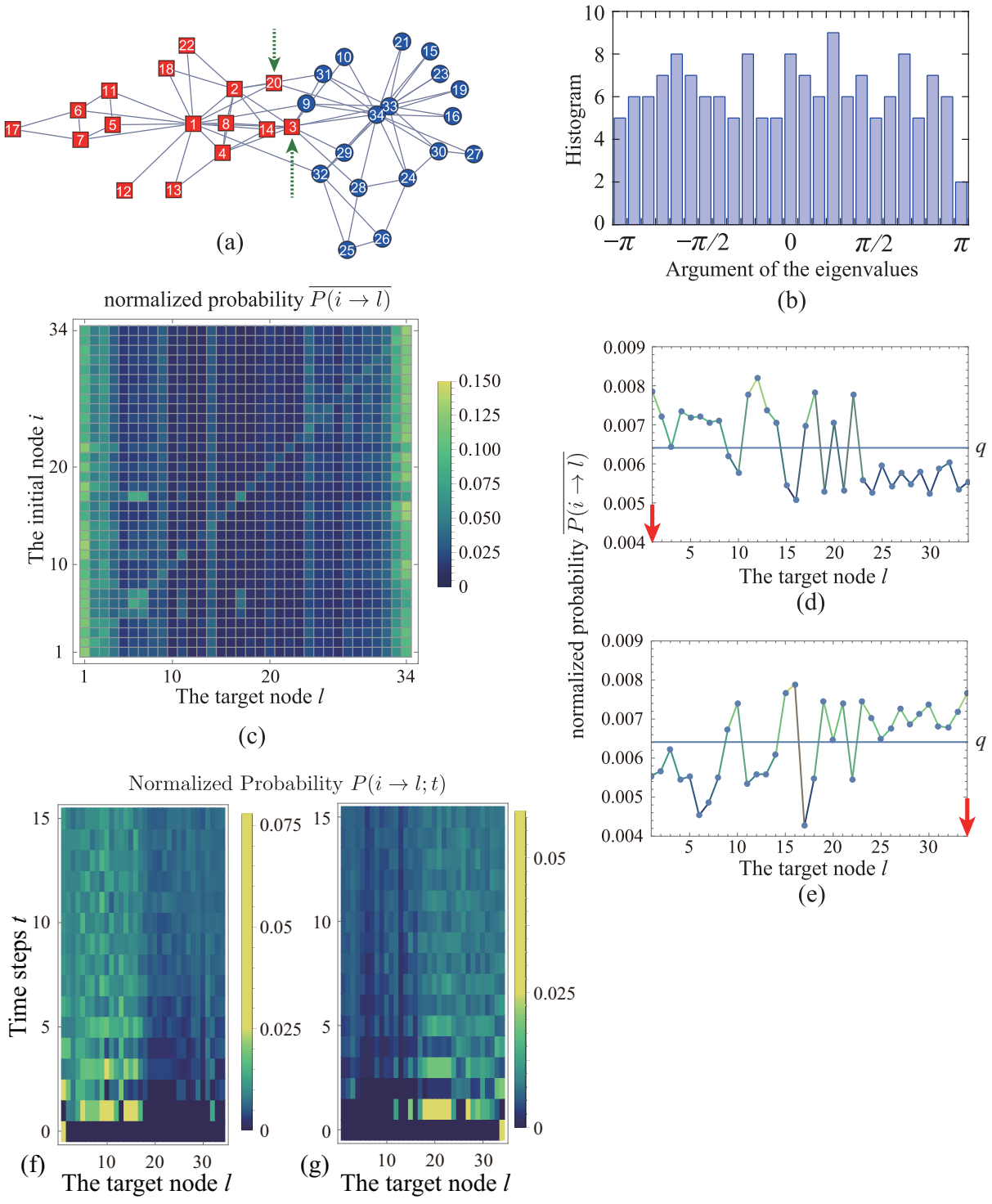

FIG. 7. (a) Zachary's karate-club network [17], for which $N = 34$ and $D = 156$. The hubs are nodes 1 and 34. The square red nodes are supposed to be in the group of node 1, and the circular blue nodes in the group of node 34. (b) Distribution of the argument of the eigenvalues of the time-evolution unitary matrix of the Fourier walk on the karate-club network. (c) Infinite-time average of the probability $\overline{p(i \to l)}$ in Eq. (15) of the Fourier walk on the karate-club network. The vertical axis shows the initial node i and the horizontal axis shows the target node l, while each square indicates the value $\overline{P(i \to l)}$. (d, e) Infinite-time average of the *normalized* probability $\overline{P(i \to l)}$ in Eq. (19) of the Fourier walk on the karate-club network that starts from the hub $i = 1$ (d) and the hub $i = 34$ (e), each of which is indicated by a red arrow. The horizontal axis shows the target node l and the vertical axis shows the normalized probability $\overline{p(i \to l)}$ with $i = 1, 34$. The horizontal line in the middle indicates the threshold $q = 1/156 \simeq 0.006\,41$. (f, g) Time evolution of the normalized probability $P(i \to l; t)$ from $t = 0$ to $t = 15$ for the Fourier walk with $i = 1$ (f) and $i = 34$ (g), where we have reordered the target nodes l so that the nodes in the first community in (a) may be gathered on the left and those in the second community on the right.

0.007 062, is markedly greater than the threshold, $q \simeq 0.006\,410$, while the latter, $\overline{P(34 \to 20)} \simeq 0.006\,451$, is only marginally greater. A slight increase in the threshold q would exclude the possibility of classifying node 20 into the community of hub 34. We thereby conclude that node 20 should belong to the community of node 1. Second, for node 3, the normalized probability $\overline{P(1 \to 3)}$ is only slightly greater than the threshold, although for node 3, $\overline{P(34 \to 3)}$ is less than the threshold.

There are indeed several views of the grouping for Zachary's network. One study [47] divided the nodes into three groups; the first is a group of node 1, the second is a group of node 34, and the third is a neutral group of nodes 9, 10, 20, 28, and 29. It is therefore reasonable that node 20 has a marginal value in Fig. 7(d). In another study [13], their algorithm classified node 3 into the group of node 34. This is consistent with our result that node 3 has a marginal value in Fig. 7(c). After all, the grouping according to the second set of answers of Zachary's experiment is based on the personal views of each subject and, hence, is not the only possible answer but remains a quite possible one.

B. U.S. Airport network

We next apply our method to the domestic airport network in the United States in 1997 [48,50] [Fig. 8(a)]. The original datum is a weighted network [48], but we use the network data as a nonweighted network. Each node in the airport network corresponds to an airport in the United States. They are connected by a link if there is a flight connection between the two airports. The total number of nodes in the airport network is $N = 332$ and the total number of links is $D = 4252$. We computed the infinite-time average, (15), of the probability of the Fourier walk by numerical diagonalization of the 4252×4252 matrix. Figure 8(b) shows that the eigenvalues of the time-evolution unitary matrix are distributed almost evenly on the unit circle of the complex plane. This validates the usage of Eq. (16).

The community structure of this airport network is *a priori* unknown, unlike the prototypical three-community network and Zachary's karate-club network. Based on the successful results above, we here use the following algorithm for community detection:

(i) We order the nodes according to the number of links k_i and regard the nodes from the top of the list as candidates for hubs.

(ii) Starting from the node i with the highest degree, which is the first candidate for the hub, we classify the nodes l whose normalized probability, (19), is higher than a threshold q, as in $\overline{P(i \to l)} > q$, into the community of hub i.

(iii) We carry out (2) repeatedly, ignoring the nodes that have been classified, until all of the nodes are classified into communities. If the node with the highest degree at the moment [e.g., node 2 in Fig. 8(c)] has already been classified into a community [e.g., the dashed green circle in Fig. 8(c)], we assume that the hub and the members of the group of the hub [e.g., the dashed orange circle in Fig. 8(c)] belong to the community into which the hub has been classified [e.g., the solid circle in Fig. 8(c)].

When we use the threshold $q = 1/D \simeq 0.000\,235\,183\,4$ as in the two cases above, we classify all the nodes into two communities, one with 260 nodes and the other with 72. As reported in Table I(a), most of the major airports are classified into the first community, while the second community contains mostly minor airports with a few exceptions.

Changing the value of the threshold q reveals the hierarchical structure of the communities as the dendrogram in Fig. 1 implies; see Fig. 8(d). We find three communities when we use the threshold q in the range $0.000\,235\,443\,4 \leqslant q \leqslant 0.000\,235\,473\,4$ [see Fig. 8(e)]. The orange circle shows the airport which belongs to the first community (147 nodes), the green square the second (151 nodes), and the blue star the third (34 nodes). Comparing the top airports in Tables I(a) and I(b), we see that many major airports in the first community in Table I(a) are distributed to the second and third communities in Table I(b).

The top airport in each community is the hub airport of the present-day major three airline companies, Chicago O'Hare for United, Dallas/Fort Worth for American, and Atlanta for Delta. We therefore claim that each of the three communities indicates the subnetwork of airline companies. Nonetheless, except for the hub airports, we see mixtures of various airlines. Note that TWA, US Airways, and America West have been merged into American, Northwest into Delta, and Continental into United. We observe that these mergers were strategically reasonable in the sense that Delta and American, respectively, merged companies that appear in communities different from their own hub airports. It would be interesting to analyze the airport network after mergers (including that of TWA into American), but it is out of the scope of the present paper.

Our algorithm of community detection can further find the hierarchy of the airline companies. By increasing the threshold further, to $q = 0.000\,235\,583\,4$, we find five communities [see Fig. 8(f)], with 109, 111, 51, 44, and 17 nodes, respectively. The fourth community (olive hexagons) splits off exactly from the second community in Fig. 8(e), and the fifth community (red ellipses) mostly from the first. We can easily see that the fourth community corresponds to Alaska Airlines [49], which is indeed a partner company of American Airlines, a major company in the second community in Fig. 8(e).

In contrast, a previous study [50] divided the airports into two communities that geographically correspond to the east and the west, the latter including the midwest. Our algorithm excels in finding a different structure since it starts from finding the hubs.

V. CONCLUSION

In the present paper, we define the discrete-time quantum walk on complex networks and utilize it for community detection. We numerically show that the Fourier walk is localized in a community to which the initial node belongs. We calculate the infinite-time average of the transition probability by the use of eigenvectors. We confirm that the eigenvectors of the Fourier walk tend to be localized in a community, while those of the Grover walk tend to be localized in some specific nodes.

We find that the infinite-time average reveals the community structure better if the eigenvalues of the unitary matrix are

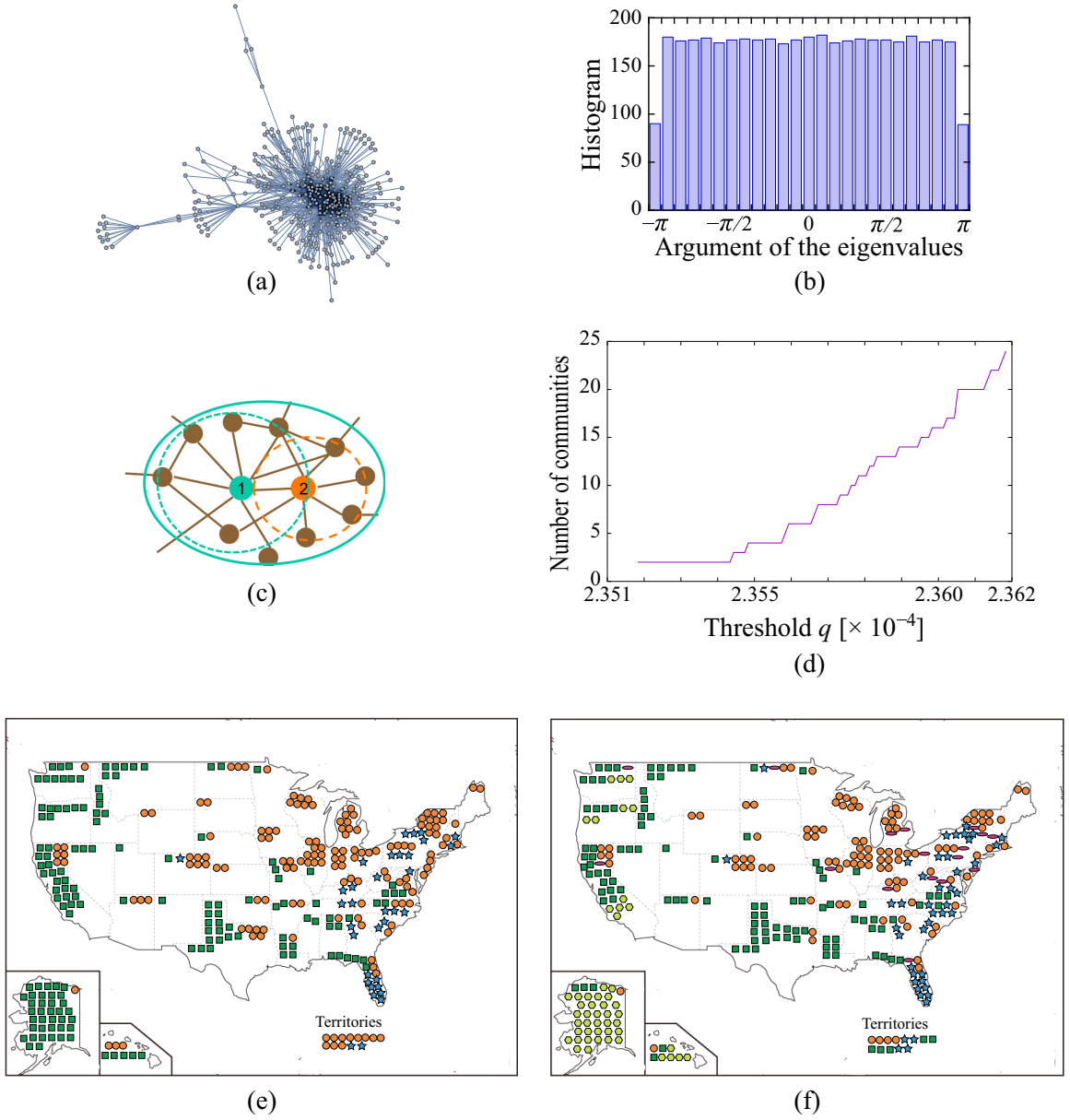

FIG. 8. (a) Airport transport network in the United States in 1997, for which $N = 332$ and $D = 4252$. (b) Distribution of the argument of the eigenvalues of the time-evolution unitary matrix for the Fourier walk on the U.S. Airport network. (c) Schematic of the community which has two hubs. Node 1 is the first hub and node 2 is classified as a member of the group (dashed green circle). Node 2 is the second hub concurrently. We classify hub 2 and its community (dashed orange circle) into the community of hub 1, ending up with a larger community (solid green circle). (d) Number of communities depending on the threshold q. The horizontal axis shows the threshold q that we set and the vertical axis shows the number of communities that we obtain. (e) Result of the community detection of the airport network. We classify the nodes into three communities when we use the threshold $q \simeq 0.000\,235\,473\,4$. The orange circle represents the airport which belongs to the first community (147 nodes). The green square shows the second one (151 nodes) and the blue star shows the third one (34 nodes). (f) Result of the community detection of the airport network. We have five communities when we use the threshold $q \simeq 0.000\,235\,583\,4$. The olive hexagon shows the airport which belongs to the fourth community, and the red ellipse the fifth.

nondegenerate, and hence the Fourier walk is more suitable for community detection than the Grover walk. The transition probability becomes higher in proportion to the number of links, and thereby we can detect the hubs. Next, we normalize the probability of each node by dividing it by the number of links. The normalized probability in the initial node and the other nodes in the same community is high, which reveals the community structure. Meanwhile, the probability of the classical random walk on the same network eventually converges to the flat distribution. We thus claim that the time average of the probability of the Fourier walk on complex networks reveals the community structure more explicitly than that of the classical random walk.

Finally, we apply the method to real-world networks. For Zachary's karate-club network, we confirm that our method reveals its community structure correctly. Most nodes of the

TABLE I. The top airports in each community according to our algorithm, along with the carrier that carried the largest number of passengers out of it. (a) For the threshold $q = 1/D \simeq 0.000\,235\,183\,4$, all airports are classified into two communities. We omit some minor airports in the second community. (b) For the threshold $0.000\,235\,443\,4 \leqslant q \leqslant 0.000\,235\,473\,4$, all airports are classified into three communities.

(a) $q = 1/D \simeq 0.000\,235\,183\,4$

First community		Second community	
Departure airport	Carrier	Departure airport	Carrier
Chicago O'Hare, IL (ORD)	United	Dallas/Fort Worth, TX (DFW)	American
Atlanta, GA (ATL)	Delta	San Francisco, CA (SFO)	United
St. Louis, MO (STL)	TWA	Salt Lake City, UT (SLC)	Delta
Pittsburgh, PA (PIT)	US Airways	Nashville, TN (BNA)	Southwest
Charlotte, NC (CLT)	US Airways	New York JFK, NJ (JFK)	American
Denver, CO (DEN)	United	Portland, OR (PDX)	Alaska
Minneapolis-St. Paul, MN (MSP)	Northwest		
Detroit, MI (DTW)	Northwest		
New York Newark, NJ (EWR)	Continental		
Philadelphia, PA (PHL)	US Airways		
Houston, TX (IAH)	Continental		
Cincinnati, OH (CVG)	Delta		
Phoenix, AZ (PHX)	America West		
Los Angeles, CA (LAX)	United		
Seattle-Tacoma, WA (SEA)	Alaska		
Orlando, FL (MCO)	Delta		
Baltimore, MD (BWI)	US Airways		
New York La Guardia, NJ (LGA)	Delta		
Raleigh, NC (RDU)	US Airways		
Boston, MA (BOS)	Delta		
Las Vegas, NV (LAS)	Southwest		
Washington Dulles, VA (IAD)	United		
Miami, FL (MIA)	American		
Cleveland, OH (CLE)	Continental		
Memphis, TN (MEM)	Northwest		
Tampa, FL (TPA)	Delta		
Washington National, VA (DCA)	US Airways		
Indianapolis, IN (IND)	US Airways		

(b) $0.000\,235\,443\,4 \leqslant q \leqslant 0.000\,235\,473\,4$

First community		Second community		Third community	
Departure airport	Airline	Departure airport	Airline	Departure airport	Airline
Chicago O'Hare, IL (ORD)	United	Dallas/Fort Worth, TX (DFW)	American	Atlanta, GA (ATL)	Delta
St. Louis, MO (STL)	TWA	Charlotte, NC (CLT)	US Airways	Philadelphia, PA (PHL)	US Airways
Pittsburgh, PA (PIT)	US Airways	Denver, CO (DEN)	United	Cincinnati, OH (CVG)	Delta
Minneapolis-St. Paul, MN (MSP)	Northwest	San Francisco, CA (SFO)	United	Orlando, FL (MCO)	Delta
Detroit, MI (DTW)	Northwest	Houston, TX (IAH)	Continental	Baltimore, MD (BWI)	US Airways
New York Newark, NJ (EWR)	Continental	Los Angeles, CA (LAX)	United	Raleigh, NC (RDU)	US Airways
Phoenix, AZ (PHX)	America West	Salt Lake City, UT (SLC)	Delta	New York La Guardia, NJ (LGA)	Delta
Boston, MA (BOS)	Delta	Seattle-Tacoma, WA (SEA)	Alaska	Miami, FL (MIA)	American
Washington Dulles, VA (IAD)	United	Nashville, TN (BNA)	Southwest	New York JFK, NJ (JFK)	American
Cleveland, OH (CLE)	Continental	Las Vegas, NV (LAS)	Southwest	Memphis, TN (MEM)	Northwest
Indianapolis, IN (IND)	US Airways	Washington National, VA (DCA)	US Airways	Tampa, FL (TPA)	Delta

network are classified clearly, while two nodes are marginally identified. This result is consistent with other research. For the airport network in the United States, we confirm that our method reveals its community structure that corresponds to the three major airline companies in the United States. By adjusting the threshold, our algorithm successfully reveals the hierarchical structure of the communities as the dendrogram in Fig. 1 implies.

We argue that the strong localization of the Grover walk is presumably due to many eigenstates of degenerate eigenvalues ± 1, which have been mathematically proven to be localized on loops [38]; hence we are almost certain that the Grover walk is not suitable for community detection. On the other hand, we numerically show that the Fourier walk works for community detection, but we have yet to find any mathematical reasons why it does. We have not tried other types of quantum walks either. These are beyond the scope of the present paper and should be pursued in future studies.

Let us, finally, add a remark on a possible extension of the present algorithm. We define our quantum walk ignoring the weight and the direction of the links of the networks. We can vary the weight as integers by making each link have multiple connections. In order for a directed network to accommodate a quantum walk, the network cannot have any dead ends of directed links [12]. We may be able to apply our algorithm to the directed network as long as the condition is satisfied.

ACKNOWLEDGMENTS

We would like to express our great appreciation to Prof. Hideaki Obuse. He taught us about quantum walks in detail and gave us extensive advice on our research. We also would like to express our great appreciation to Prof. Masaki Sano and Prof. Takeo Kato, who made many helpful comments. We also would like to thank many people for many discussions at our poster presentation. The present study was partially supported by Japan Society for the Promotion of Science (JSPS) Grant-in-Aid for Scientific Research (KAKENHI) (A) No. 19H00658.

APPENDIX A: TRANSFORMATION TO THE STANDARD SHIFT OPERATOR

In the present Appendix, we explicitly show for a one-dimensional lattice that we can transform the atypical shift operator, (8), to the standard shift operator by multiplying the coin operator by the flipping operator.

Following the text, let us express the right- and left-movers on the one-dimensional lattice as follows:

$$\begin{aligned}\text{Right mover:}\quad &\ldots, |(x-1)\to x\rangle,\\ &|x\to(x+1)\rangle,\\ &|(x+1)\to(x+2)\rangle,\ldots,\end{aligned}\tag{A1}$$

$$\begin{aligned}\text{Left mover:}\quad &\ldots, |(x+2)\to(x+1)\rangle,\\ &|(x+1)\to x\rangle,\\ &|x\to(x-1)\rangle\ldots.\end{aligned}\tag{A2}$$

We can express the atypical shift operator, (8), in the form of the matrix

$$S=\left(\begin{array}{c|c|c|c|c}
\ddots & 1 & & & \\ \hline
1 & & 1 & & \\ \hline
 & 1 & & 1 & \\ \hline
 & & 1 & & 1 \\ \hline
 & & & 1 & \ddots
\end{array}\right)\tag{A3}$$

under the ordering of the bases

$$\left(\begin{array}{c}
\vdots \\ \hline
|(x-1)\to(x-2)\rangle \\
|(x-1)\to x\rangle \\ \hline
|x\to(x-1)\rangle \\
|x\to(x+1)\rangle \\ \hline
|(x+1)\to x\rangle \\
|(x+1)\to(x+2)\rangle \\ \hline
\vdots
\end{array}\right)\tag{A4}$$

because

$$\begin{aligned}
S|x\to(x-1)\rangle &= |(x-1)\to x\rangle,\\
S|(x-1)\to x\rangle &= |x\to(x-1)\rangle,\\
S|(x+1)\to x\rangle &= |x\to(x+1)\rangle,\\
S|x\to(x+1)\rangle &= |(x+1)\to x\rangle.
\end{aligned}\tag{A5}$$

The time-evolution unitary operator is therefore given by

$$U = SC\tag{A6}$$

with the coin operator

$$C = \ldots\oplus C_{x-1}\oplus C_x\oplus C_{x+1}\ldots\tag{A7}$$

with a 2×2 unitary matrix C_x, for example, a Fourier coin,

$$C_x=\frac{1}{\sqrt{2}}\begin{pmatrix}1 & 1\\ 1 & -1\end{pmatrix}.\tag{A8}$$

We now define a new coin operator with an additional factor P_x inserted to the left of the original coin operator C_x,

$$C' = PC = \ldots\oplus P_{x-1}C_{x-1}\oplus P_xC_x\oplus P_{x+1}C_{x+1}\ldots,\tag{A9}$$

where the new factor

$$P_x=\begin{pmatrix}0 & 1\\ 1 & 0\end{pmatrix}\tag{A10}$$

flips the direction of the right- and left-movers. In the new time-evolution operator

$$U' = SC' = SPC,\tag{A11}$$

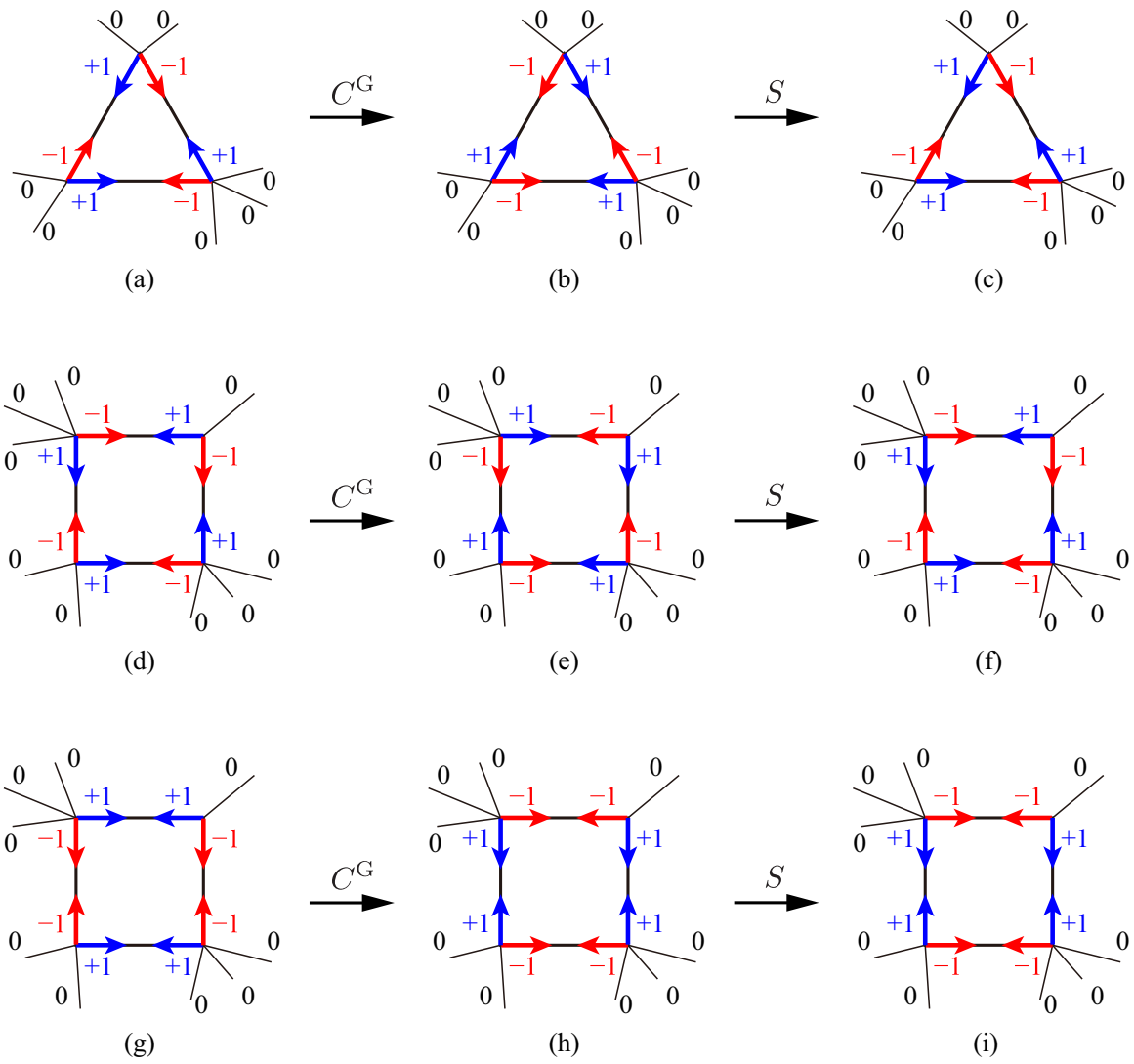

FIG. 9. (a–c) An eigenvector of the Grover walk on a graph, which is localized on a triangular loop, has the eigenvalue $+1$. (d–f) An eigenvector localized on a square loop also has the eigenvalue $+1$. (g–i) Another eigenvector localized on a square loop has the eigenvalue -1.

we find

$$S' = SP = \begin{pmatrix} \ddots & 1 & & & \\ & & 1 & & \\ & 1 & & & \\ & & & 1 & \\ & & 1 & & \\ & & & 1 & \ddots \end{pmatrix}, \tag{A12}$$

because

$$\begin{aligned} S'|x \to (x+1)\rangle &= S|x \to (x-1)\rangle = |(x-1) \to x\rangle, \\ S'|(x-1) \to (x-2)\rangle &= S|(x-1) \to x\rangle = |x \to (x-1)\rangle, \\ S'|(x+1) \to (x+2)\rangle &= S|(x+1) \to x\rangle = |x \to (x+1)\rangle, \\ S'|x \to (x-1)\rangle &= S|x \to (x+1)\rangle = |(x+1) \to x\rangle. \end{aligned} \tag{A13}$$

We can see that the operator S' works as the standard shift operator, which shifts the right-mover to the right, keeping it as a right-mover, and shifts the left-mover to the left, keeping it as a left-mover.

Therefore, the time-evolution operator

$$U' = SC' = S'C \tag{A14}$$

is the atypical shift operator, (8), multiplied by a slightly jammed coin operator; for example, for Eq. (A8),

$$C'_x = PC_x = \frac{1}{\sqrt{2}}\begin{pmatrix} 1 & -1 \\ 1 & 1 \end{pmatrix} \tag{A15}$$

but, at the same time, is the standard shift operator S' multiplied by the standard coin operator C. In this sense, the atypical shift operator, (8), is quite similar to the standard shift operator.

APPENDIX B: EIGENVECTORS OF THE GROVER WALK ON GRAPHS FOR THE EIGENVALUES ±1

We here present tutorial examples of the eigenvectors of the Grover walk on graphs for the degenerate eigenvalues ±1. The following is based on private discussions with H. Obuse [51] and E. Segawa [52].

Let us first note that the Grover coin C_i^{G} in Eq. (11) always has an eigenvalue of -1 for an eigenvector with only two nonzero elements. We can straightforwardly confirm it by applying the Grover coin to the vector $(1 \quad -1 \quad 0 \quad 0 \quad \ldots)^T$:

$$\frac{1}{k_i}\begin{pmatrix} 2-k_i & 2 & 2 & 2 & 2 \\ 2 & 2-k_i & 2 & 2 & 2 \\ 2 & 2 & 2-k_i & 2 & 2 \\ \vdots & \vdots & \vdots & \ddots & \vdots \\ 2 & 2 & 2 & \cdots & 2-k_i \end{pmatrix}\begin{pmatrix} 1 \\ -1 \\ 0 \\ \vdots \\ 0 \end{pmatrix} = \begin{pmatrix} -1 \\ 1 \\ 0 \\ \vdots \\ 0 \end{pmatrix}. \tag{B1}$$

We first show [51] that the vector depicted in Fig. 9(a) is an eigenvector of the Grover walk with the eigenvalue $+1$. There the blue arrow with the sign $+1$ indicates that the vector has an element $+1$ for the basis at the node to which the arrow is attached and is about to hop to the next node. The red arrow with the sign -1 indicates an element -1 for the corresponding basis. The other elements are all 0. In other words, this vector is strictly localized on a triangular loop.

Application of the Grover coin to the vector changes it to the one depicted in Fig. 9(b) because of the operation in Eq. (B1). Further application of the shift operator in Eq. (8) changes it back to the original one as in Fig. 9(c). We have thereby confirmed that the vector in Fig. 9(a) is an eigenvector of the Grover walk with the eigenvalue $+1$.

We can confirm in the same way that the vector depicted in Fig. 9(d), localized strictly on a square loop, is also an eigenvector of the Grover walk with the eigenvalue $+1$. On a square loop, we can find that another vector, depicted in Fig. 9(g), is an eigenvector of the Grover walk but with the eigenvalue -1. We can thus easily guess that the Grover walk must have large degrees of degeneracies for the eigenvalues ±1.

Indeed, it has been proven [38,52] for the Grover walk on a graph G that the degeneracy of the eigenvalue $+1$ is $b_1(G)+1$, whereas the degeneracy of the eigenvalue -1 is $b_1(G)+1$ if the graph G is bipartite and $b_1(G)-1$ if it is not, where $b_1(G) = |E| - |V| + 1$ is the Betti number of the graph G, with $|E|$ and $|V|$ denoting the number of edges (links) and vertices (nodes), respectively.

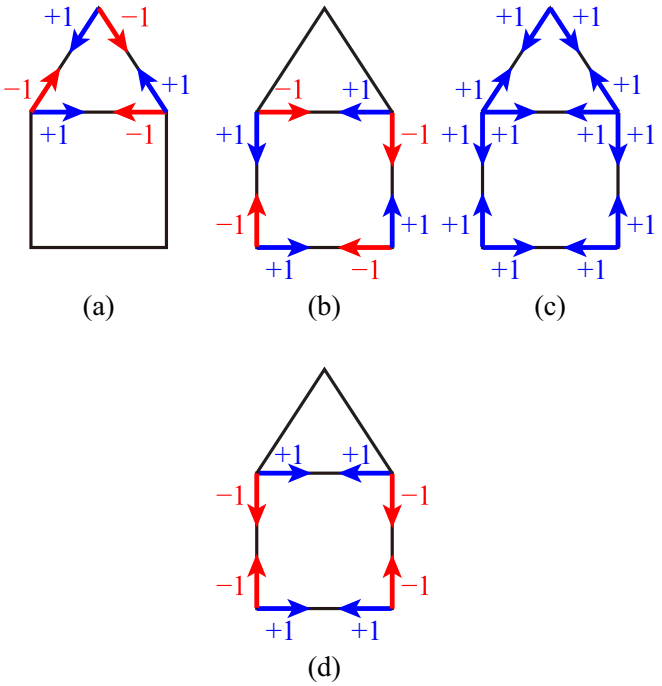

FIG. 10. (a–c) The three eigenvectors degenerate to the eigenvalue $+1$. (d) The only eigenvector with the eigenvalue -1.

We can easily confirm this, e.g., for the graph in Fig. 10, which is a combination of a square and a triangle with the Betti number $b_1(G) = 6 - 5 + 1 = 2$. According to the theorem, the degeneracies of the eigenvalues ±1 are $b_1(G)+1 = 3$ and $b_1(G)-1 = 1$, respectively, because the graph is not bipartite. Indeed, the vectors depicted in Figs. 10(a)–10(c) have the eigenvalue $+1$, while the vector in Fig. 10(d) has the eigenvalue -1.

Note that although there is always an extended eigenvector, such as exemplified in Fig. 10(c), namely, the same element in all bases, with the eigenvalue $+1$, its overlap with the initial state of the Grover walk should be of the order of $1/\sqrt{D}$ because of the normalization of the eigenvector, and hence we can ignore its contribution for large networks.

For the three-community network in Fig. 3(a), because the Betti number is given by $b_1(G) = 39 - 21 + 1 = 19$, the degeneracies in the eigenvalues ±1 are 20 and 18, respectively. For Zhachary's karate club in Fig. 7(a), they are 46 and 44, and for the airport transport network in Fig. 8(a), they are 1796 and 1794. Except for the one extended eigenvector, they are all localized on loops in at least one set of linear combinations of degenerate eigenvectors.

[1] Y. Aharonov, L. Davidovich, and N. Zagury, Quantum random walks, Phys. Rev. A **48**, 1687 (1993).

[2] E. Farhi and S. Gutmann, Quantum computation and decision trees, Phys. Rev. A **58**, 915 (1998).

[3] D. Aharonov, A. Ambainis, J. Kempe, and U. V. Vazirani, Quantum walks on graphs, in *Proceedings of the 33rd Annual ACM Symposium on Theory of Computing* (Association for Computing Machinery, New York, 2001), pp. 50–59.

[4] N. Inui, N. Konnno, and E. Segawa, One-dimensional three-state quantum walk, Phys. Rev. E **72**, 056112 (2005).

[5] T. Machida, Limit theorems for a localization model of 2-state quantum walk, Int. J. Quant. Info. **9**, 863 (2011).

[6] A. C. Oliveira, R. Portugal, and R. Donangelo, Decoherence in two-dimensional quantum walks, Phys. Rev. A **74**, 012312 (2006).

[7] K. Saito, Periodicity for the Fourier quantum walk on regular graphs, Quantum Info. Comput. **19**, 23 (2019).

[8] L. Grover, A fast quantum mechanical algorithm for database search, in *Proceedings of the 28th Annual ACM Symposium on Theory of Computing* (Association for Computing Machinery, New York, 1996), pp. 212–219.

[9] S. D. Berry and J. B. Wang, Quantum-walk-based search and centrality, Phys. Rev. A **82**, 042333 (2010).

[10] B. C. Travaglione and G. J. Milburn, Implementing the quantum random walk, Phys. Rev. A **65**, 032310 (2002).

[11] A. Crespi, R. Osellame, R. Ramponi, M. Bentivegna, F. Flamini, N. Spagnolo, N. Viggianiello, L. Innocenti, P. Mataloni, and F. Sciarrino, Suppression law of quantum states in a 3D photonic fast Fourier transform chip, Nat. Commun. **7**, 10469 (2016).

[12] A. Montanaro, Quantum walks on directed graphs, Quantum Info. Comput. **7**, 93 (2007).

[13] M. Girvan and M. E. J. Newman, Community structure in social and biological networks, Proc. Natl. Acad. Sci. USA **99**, 7821 (2002).

[14] E. Estrada, *The Structure of Complex Networks: Theory and Applications* (Oxford University Press, Oxford, UK, 2011).

[15] G. Chen, X. Wang, and X. Li, *Fundamentals of Complex Networks: Models, Structures and Dynamics* (John Wiley & Sons, Singapore, 2015).

[16] V. Latora, V. Nicosia, and G. Russo, *Complex Networks: Principles, Methods and Applications* (Cambridge University Press, Cambridge, UK, 2017).

[17] W. W. Zachary, An information flow model for conflict and fission in small groups, J. Anthropol. Res. **33**, 452 (1977).

[18] G. W. Flake, S. Lawrence, C. Lee Giles, and F. M. Coetzee, Self-organization and identification of web communities, IEEE Comput. **35**, 66 (2002).

[19] M. Takayasu, S. Sameshima, T. Ohnishi, Y. Ikeda, H. Takayasu, and K. Watanabe, Massive economics data analysis by econophysics methods—The case of companies' network structure, in *Annual Report of the Earth Simulator Center April 2007–March 2008* (Earth Simulator Center, Japan Agency for Marine-Earth Science and Technology, Yokohama, 2008), pp. 263–268.

[20] D. J. Watts and S. H. Strogatz, Collective dynamics of 'small-world' networks, Nature (London) **393**, 440 (1998).

[21] R. J. Williams and N. D. Martinez, Simple rules yield complex food webs, Nature (London) **404**, 180 (2000).

[22] A. W. Rives and T. Galitski, Modular organization of cellular networks, Proc. Natl. Acad. Sci. USA **100**, 1128 (2003).

[23] S. H. Strogatz, Exploring complex networks, Nature (London) **410**, 268 (2001).

[24] S. Milgram, The small world problem, Psychol. Today **2**, 60 (1967).

[25] F. Radicchi, C. Castellano, F. Cecconi, V. Loreto, and D. Parisi, Defining and identifying communities in networks, Proc. Natl. Acad. Sci. USA **101**, 2658 (2004).

[26] S. Fortunato, Community detection in graphs, Phys. Rep. **486**, 75 (2010).

[27] M. E. J. Newman, Finding community structure in networks using the eigenvectors of matrices, Phys. Rev. E **74**, 036104 (2006).

[28] P. Pons and M. Latapy, *Computing Communities in Large Networks Using Random Walks* (Springer, New York, 2005), pp. 284–293.

[29] T. Hastie, R. Tibshirani, and J. H. Friedman, *The Elements of Statistical Learning* (Springer, Berlin, 2001).

[30] E. Estrada and N. Hatano, Communicability in complex networks, Phys. Rev. E **77**, 036111 (2008).

[31] M. E. J. Newman, Modularity and community structure in networks, Proc. Natl. Acad. Sci. USA **103**, 8577 (2006).

[32] A. Clauset, M. E. J. Newman, and C. Moore, Finding community structure in very large networks, Phys. Rev. E **70**, 066111 (2004).

[33] M. Rosvall and C. T. Bergstrom, Maps of random walks on complex networks reveal community structure, Proc. Natl. Acad. Sci. USA **105**, 1118 (2008).

[34] A. M. C. Souza and R. F. S. Andrade, Discrete time quantum walk on the Apollonian network, J. Phys. A: Math. Theor. **46**, 145102 (2013).

[35] N. Shenvi, J. Kempe, and K. B. Whaley, Quantum random-walk search algorithm, Phys. Rev. A **67**, 052307 (2003).

[36] Y. Higuchi, N. Konno, I. Sato, and E. Sagawa, Periodicity of the discrete-time quantum walk on a finite graph, Interdiscip. Info. Sci. **23**, 75 (2017).

[37] Y. Ide, N. Konno, and E. Segawa, Time averaged distribution of a discrete-time quantum walk on the path, Quantum Info. Process. **11**, 1207 (2012).

[38] Y. Higuchi, N. Konno, I. Sato, and E. Segawa, Spectral and asymptotic properties of Grover walks on crystal lattices, J. Func. Anal. **267**, 4197 (2014).

[39] P. Pradhan, A. Yadav, S. K. Dwivedi, and S. Jalan, Optimized evolution of networks for principal eigenvector localization, Phys. Rev. E **96**, 022312 (2017).

[40] A. V. Goltsev, S. N. Dorogovtsev, J. G. Oliveira, and J. F. F. Mendes, Localization and Spreading of Diseases in Complex Networks, Phys. Rev. Lett. **109**, 128702 (2012).

[41] P. W. Anderson, Absence of diffusion in certain random lattices, Phys. Rev. **109**, 1492 (1958).

[42] T. Devakul and D. A. Huse, Anderson localization transitions with and without random potentials, Phys. Rev. B **96**, 214201 (2017).

[43] I. Vakulchyk, M. V. Fistul, P. Qin, and S. Flach, Anderson localization in generalized discrete time quantum walks, Phys. Rev. B **96**, 144204 (2017).

[44] S. Derevyanko, Anderson localization of a one-dimensional quantum walker, Sci. Rep. **8**, 1795 (2018).

[45] N. Inui, Y. Konishi, and N. Konno, Localization of two-dimensional quantum walks, Phys. Rev. A **69**, 052323 (2004).

[46] T. Komatsu and T. Tate, Eigenvalues of quantum walks of Grover and Fourier types, J. Fourier Anal. Appl. **25**, 1293 (2019).

[47] H. Wu, L. Gao, J. Dong, and X. Jang, Detecting overlapping protein complexes by rough-fuzzy clustering in protein-protein networks, PLOS ONE **9**, e91856 (2014).

[48] V. Batagelj and A. Mrvar, Pajek datasets; http://vlado.fmf.uni-lj.si/pub/networks/data/.

[49] Bureau of Transportation Statistics, https://www.transtats.bts.gov/DL_SelectFields.asp.

[50] E. Estrada and N. Hatano, Communicability graph and community structures in complex networks, Appl. Math. Comput. **214**, 500 (2009).

[51] H. Obuse (private communication, 2019).

[52] E. Segawa (private communication, 2019).